Influence of microstructure on the magnetic and mechanical behaviour of amorphous and nanocrystalline FeNbB alloy

2002 J. Phys.: Condens. Matter 14 4717

(http://iopscience.iop.org/0953-8984/14/18/307)

INSTITUTE OF PHYSICS PUBLISHING JOURNAL OF PHYSICS: CONDENSED MATTER

J. Phys.: Condens. Matter **14** (2002) 4717–4736 PII: S0953-8984(02)32990-4

Influence of microstructure on the magnetic and mechanical behaviour of amorphous and nanocrystalline FeNbB alloy

I Škorvánek[1,5], P Švec[2], J-M Grenèche[3], J Kováč[1], J Marcin[1] and R Gerling[4]

[1] Institute of Experimental Physics, Slovak Academy of Sciences, Watsonova 47, 043 53 Košice, Slovakia
[2] Institute of Physics, Slovak Academy of Sciences, Dúbravská cesta 9, 842 28 Bratislava, Slovakia
[3] Laboratoire de Physique de l'Etat Condensé, UMR CNRS 6087, Université du Maine, Faculté des Sciences, 72085 Le Mans Cedex 9, France
[4] GKSS-Forschungszentrum Geesthacht GmbH, Institut für Werkstoffforschung, Postfach 1160, D-21494 Geesthacht, Germany

E-mail: skorvi@saske.sk

Received 24 January 2002, in final form 13 March 2002
Published 26 April 2002
Online at stacks.iop.org/JPhysCM/14/4717

Abstract

The formation of a nanocrystalline structure and its influence on the magnetic and mechanical properties in a ternary $Fe_{80.5}Nb_7B_{12.5}$ alloy has been investigated using a variety of complementary methods. The crystallization studies performed by DSC calorimetry, magnetization and electrical resistivity measurements have confirmed a two-stage nature of the primary crystallization process. The microstructure in the series of heat-treated amorphous and nanocrystalline specimens with different volume fractions of crystalline phase was examined by transmission electron microscopy, x-ray diffraction and ^{57}Fe Mössbauer spectrometry. The results obtained by a combination of static magnetic measurements and Mössbauer spectrometry have indicated a higher degree of structural and magnetic inhomogeneity of the residual amorphous phase after nanocrystallization. Striking differences in the magnetic hardening regime at elevated temperatures have been observed for the samples with different volume fractions of nanocrystalline particles. The strongest magnetic hardening effects are visible for the samples exhibiting a medium degree of crystallinity, while the best soft-magnetic properties are obtained for the samples where the primary crystallization process is nearly finished. The ductility tests have revealed that the transition from ductile to brittle behaviour develops predominantly in an amorphous phase just before crystallization and the subsequent crystallization causes only slight changes in the embrittlement level. On the other hand, the hardness is rather insensitive to the structural relaxation processes before crystallization and its value increases proportionally to the volume fraction of precipitated nanocrystalline grains.

[5] Author to whom any correspondence should be addressed.

0953-8984/02/184717+20$30.00

1. Introduction

Fe-based nanocrystalline alloys prepared by the controlled crystallization of melt-spun amorphous precursors have been an object of intense research over the last decade. The particular interest in these alloys results from their excellent soft-magnetic properties. The most widely studied alloy system of this group is $Fe_{73.5}Cu_1Nb_3Si_{13.5}B_9$, also known under the commercial name Finemet [1]. Among the nanocrystalline alloys developed more recently, the Fe–M–B–(Cu)-type alloys (M = Zr, Hf and Nb) are also attractive because of the simplicity of the alloy system as well as the high saturation magnetization values (1.5–1.7 T) [2]. The alloys of this soft-magnetic nanocrystalline material group, called also Nanoperm, have good prospects to be used in various soft-magnetic applications [3].

The excellent magnetic properties of these nanocrystalline systems arise from the fact that the bcc-Fe nanocrystallites with grain size smaller than the exchange length are strongly exchange coupled via the surrounding amorphous interphase regions, which leads to the averaging out of the magnetic anisotropy of the individual crystalline grains [4]. Moreover, the development of nanocrystalline structure leads to a considerable decrease of the saturation magnetostriction [5].

An important factor, which should be considered for the soft-magnetic applications, is the strength and the temperature dependence of the exchange coupling between the nanocrystalline grains mediated by the intergranular amorphous matrix phase. The Curie temperature of the residual amorphous matrix, T_c(am), is generally lower than that of the nanocrystalline phase. The nanograins are well coupled magnetically via the remaining amorphous matrix far below T_c(am). On the other hand, at temperatures close to and/or above T_c(am) the weak magnetic matrix does not enable good exchange coupling between grains, and therefore the magnetic properties are deteriorated. For a better description of the effects of magnetic coupling between grains, the original single-phase effective anisotropy model [4] has been extended towards two-phase models by Herzer [5], Hernando *et al* [6] and Suzuki and Cadogan [7]. The resulting phenomenological models allowed us to explain the magnetic hardening observed during the first stages of nanocrystallization, where the nanocrystals are separated by relatively thick amorphous matrix [6,8], as well as the magnetic hardening experimentally observed at elevated temperatures, when the measuring temperatures approach T_c(am) [9–11].

Among the most significant structural parameters which govern the physical properties in these nanocrystalline alloys are the size and the volume fraction of the crystalline grains as well as the microstructural and chemical nature of the intergranular amorphous phase. Therefore, in order to optimize the properties of the particular nanocrystalline material for desired applications it is important to understand in more detail the processes which control the development of the microstructure during annealing. In this context, the primary crystallization process is of particular interest. In the case of Nanoperm alloys one usually distinguishes two scenarios [12]:

(i) one stage with a nucleation-and-growth mechanism as observed typically in FeZrB(Cu) alloys and
(ii) two different kinetic stages where nucleation-and-growth and grain-growth mechanisms take place, respectively, as observed in some Cu-free FeNbB nanocrystalline alloys. In contrast to the numerous experimental studies of the interplay between the microstructure and magnetic properties of FeZrB(Cu) alloys, such studies using FeNbB nanocrystalline alloys with a two-stage primary crystallization regime have been less intense.

The major hindrance to widespread massive technological applications of nanocrystalline ferromagnetic materials arises from their brittleness, induced during the development of the

crystalline phase in the heat treatment process. Its origin has not yet been fully understood. The results of some investigations undertaken in this respect on Finemet alloys have clearly shown that the embrittlement occurs predominantly prior to nanocrystallization, i.e. still in the amorphous phase, being most probably related to some atomic rearrangements in amorphous structure [13–15]. Some improvement in the ductility of nanocrystalline Finemet alloys has been reported by Allia *et al* [15, 16] after application of fast dc-Joule heating treatments in vacuum. It is assumed that by this treatment, the embrittlement is mitigated by more rapid development of nanostructure.

There is a lack of experimental studies dealing with the evolution of mechanical properties in the Nanoperm alloys. Hence, in addition to the magnetic characterization, there exists a clear need to investigate in more detail the ductile/brittle transformation in these systems because ductility is one of the key issues for the manufacturability and performance of engineering materials.

The aim of this work is to study the correlation between microstructure and the magnetic and mechanical properties in nanocrystalline $Fe_{80.5}Nb_7B_{12.5}$. By different heat treatments, a set of amorphous and nanocrystalline samples was prepared and characterized by x-ray diffraction, transmission electron microscopy (TEM), electrical resistivity, vibrating sample magnetometer (VSM), hysteresis loop measurements and ductility and microhardness tests, giving an insight into the structural, magnetic and mechanical properties, respectively. In addition, ^{57}Fe Mössbauer spectrometry provided relevant structural and magnetic data on each of the present phases, thanks to its local probe character.

This combination of a variety of complementary methods provides a deeper insight in the magnetic behaviour at temperatures close to and above the Curie temperature of the residual amorphous matrix that differs significantly according to the crystalline content. Special attention has been given to the role of the heat-treatment-induced structural changes in the amorphous phase on the magnetic behaviour and the embrittlement process.

2. Experimental section

Master alloys have been prepared from elements with purity better than 99.8% in a vacuum induction furnace. Amorphous ribbons 10 mm wide and 30 μm thick have been prepared by a planar flow casting method from the melt. Pieces of these ribbons were annealed under a protective argon atmosphere for 1 h at temperatures ranging from 473 to 943 K in order to prepare a representative set of relaxed amorphous and nanocrystalline samples characterized by different microstructures.

The crystallization behaviour of the samples was investigated by differential scanning calorimetry. Thermal data were measured at a heating rate of 10 K min^{-1}. The changes in microstructure upon annealing were examined by transmission electron microscopy (TEM) and by x-ray diffraction analysis (XRD). The x-ray measurements were performed using Cu Kα radiation in Bragg–Brentano configuration with a graphite monochromator in the diffracted beam. X-ray spectra were taken at 2θ steps of 0.1 angular degree and fine-scale scans in the vicinity of the diffraction peaks were performed using 0.002° steps for accurate determination of the lattice parameter of the crystalline phase(s). Samples for transmission electron microscopy were thinned, after corresponding heat treatment, by ion beam milling; TEM and electron diffraction observations were performed using a JEM1200 EX microscope.

Measurements of the saturation magnetization in series of investigated samples have been performed by using VSM-magnetometry over the temperature range from 4.2 to 1050 K. Thermomagnetic scans were obtained at a heating rate of 10 K min^{-1}. Electrical resistivity was measured using the high-precision four-probe method during linear heating with rates

of 7 and 33 K min^{-1} and in the isothermal regime with the long-term stability of the annealing temperature better than 0.1 K. The coercivity was measured using a quasi-static B–H loop tracer in the temperature range from 77 to 800 K.

^{57}Fe Mössbauer experiments were performed in transmission geometry using a conventional spectrometer with a constant acceleration signal and a ^{57}Co source diffused into a rhodium matrix. The samples were located under vacuum in either a bath cryostat or a cryofurnace to carry out spectral measurements at temperatures comprised between 77 and 800 K. After high-temperature measurements the Mössbauer spectra were systematically collected again at 77 or 300 K in order to check the occurrence of any further structural transformation. Samples were maintained perpendicular to the unpolarized γ-beam to obtain Mössbauer spectra but some texture-free spectra were also obtained using the magic angle configuration to check the effect of the ferromagnetic texture.

The analysis of Mössbauer spectra was performed using the Mosfit program [17]. The values of isomer shift were quoted relative to that of bcc-Fe at 300 K. In the case of amorphous alloys, the description only consists in a discrete distribution of hyperfine field or of quadrupolar splitting linearly correlated with that of isomer shift, below and above the Curie point of the as-quenched amorphous alloy, respectively. The spectra of nanocrystalline samples are analysed by considering three main components:

(i) the sextet with sharp lines attributed to the crystalline grains;
(ii) the contribution with broad lines located in the internal wings of external lines of the previous component assigned to the crystalline/amorphous interfacial zones;
(iii) the broad-line sextet at low temperatures which progressively collapses into a broad-line central quadrupolar doublet at high temperatures due to the intergranular phase.

The first component was described using a single sextet with free parameters and the second one with a discrete distribution of hyperfine fields, while the latter one resulted from either a discrete distribution of hyperfine field or quadrupolar splitting linearly correlated to that of isomer shift. Details of the refinement procedure were reported in [18].

The ductile/brittle behaviour of the thermally treated samples was studied by two different methods. The relative strain at fracture (ε_f) was determined by using simple bending tests. Here the sample has been bent into a U-shape between two parallel plates, the separation of which decreased until fracture occurred. From the separation of the parallel plates at failure and the thickness of the ribbon, the relative strain at fracture can be calculated [19]. The elongation of the ribbon to failure (ε_{BP}) is determined by miniaturized ball punch tests using a ball of 2.5 mm and a die of 4 mm in diameter [20]. As an additional method to study the mechanical properties of differently heat-treated samples we have employed microhardness tests. The measurements have been performed by using a Fischerscope® H100 hardness tester. Prior to the measurements the samples were embedded in artificial resin and mechanically ground and polished. Within a time of 15 s the indentation load was increased from 0 to 1 N and this load was then maintained for an additional 10 s. One hardness value was determined from ten indentations. The indentations were made in the direction parallel to the length and perpendicular to the width and thickness of the ribbon. The morphology of the indentations was characterized by light optical microscopy.

3. Results

3.1. Crystallization behaviour

The DSC thermogram of the as-quenched sample (see figure 1) shows a three-step crystallization process. As confirmed by x-ray diffraction, the first crystallization step

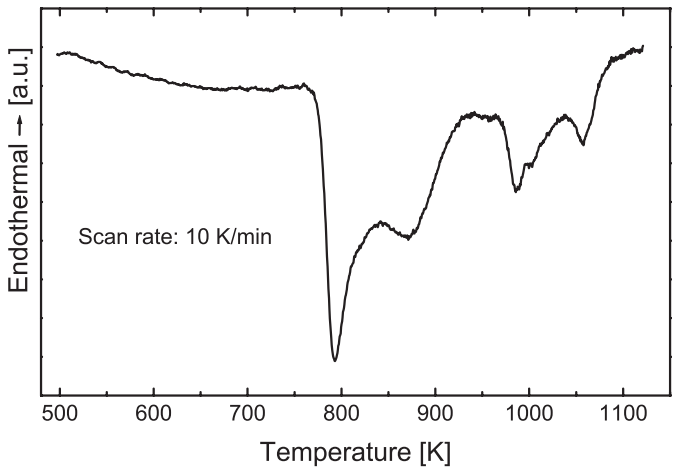

Figure 1. DSC thermogram of the amorphous $Fe_{80.5}Nb_7B_{12.5}$ sample obtained at the heating rate 10 K min^{-1}.

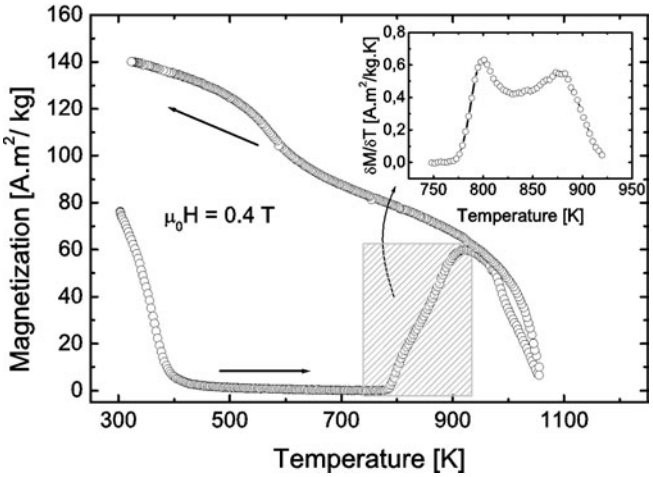

Figure 2. Thermomagnetic plot obtained at the heating rate 10 K min^{-1}. The inset shows the first derivative of magnetization with temperature in the indicated area.

characterized by the exothermic reaction with the overlapped double-peak structure (the onset at $T_{x1} = 776$ K and the peak positions detected at $T_{p1} = 793$ K and $T_{p1'} = 886$ K) corresponds to the formation of the nanocrystalline bcc-Fe phase. The bimodal character of the first crystallization step clearly indicates the two-stage nature of the primary crystallization process, which was reported for the FeNbB alloy of similar composition by Suzuki *et al* [21]. The second and the third crystallization steps indicated by DSC peaks above 950 K are associated with the formation of other crystalline phases (Fe and Nb borides). These latter stages of crystallization are characterized by a deterioration of good soft-magnetic characteristics, and, hence, they are not of interest for our study.

Figure 2 shows the temperature dependence of magnetization for the as-quenched sample measured at an applied field of 0.4 T by using VSM. The first fall of magnetization after heating of amorphous material corresponds to the ferro–paramagnetic transition of the amorphous

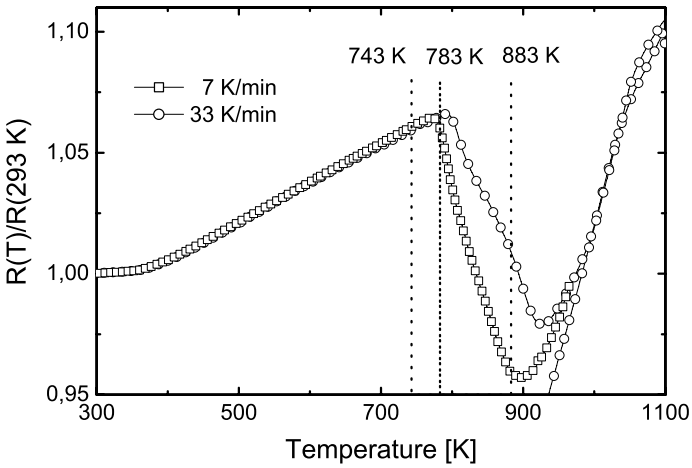

Figure 3. Temperature dependence of electrical resistivity of the $Fe_{80.5}Nb_7B_{12.5}$ samples, heating rates 7 and 33 K min^{-1}. The vertical dotted lines indicate the temperatures at which the samples for more detailed analysis were annealed.

alloy with T_c(am) $\approx$ 365 K. The increase of magnetization at 775 K indicates the onset of crystallization, where the ferromagnetic bcc-Fe grains with the Curie temperature higher than the measuring temperature are formed. Since the amorphous phase is paramagnetic in this temperature range, the magnetization is a direct measure of the respective volume fraction of the crystalline phase that has been formed due to amorphous–crystalline transformation. As we have used a constant heating rate of 10 K min^{-1}, the change in the volume fraction of bcc-Fe phase with temperature can be estimated as a derivative of magnetization in that temperature range where the crystallization takes place (see the marked area and inset in figure 2). The result of such a procedure is given in the inset of figure 2. The two-stage primary crystallization process can be clearly distinguished and a very good agreement with the DSC results is reflected by a noticeable coincidence between positions of the respective peaks and the onset of crystallization. Hence, in this case magnetometry can compete well with the classical thermal calorimetry methods.

The temperature dependence of the electrical resistivity for two different heating rates, 7 and 33 K min^{-1}, upon heating and cooling is shown in figure 3. The change of slope at around 370 K can be assigned to the ferromagnetic/paramagnetic transition of the amorphous sample. A decrease in resistivity around 770 K correlates well with the onset of crystallization. The decrease exhibits a suggestion of bimodality, which is accentuated by a faster heating rate.

The crystallization is completed above 900 K; recrystallization of the devitrified sample takes place in the vicinity of 970 K, as indicated by a kink in the resistivity curve and an irreversible behaviour upon cooling in this temperature region, where a formation of pure polycrystalline α-Fe and orthorhombic $(FeNb)_3B$ borides occurs [22].

Upon isothermal annealing the electrical resistivity decreases (see figure 4); the decrease, however, is not a simple sigmoidal dependence. At lower temperatures (between 743 and 823 K) the decrease is slow and the crystallization process is far from completed even after long-time annealing ($\sim$1000 min). At temperatures between 823 and 903 K the process exhibits an initial decrease due to the formation of the nanocrystalline particles with a diameter of about 10 nm, as confirmed by TEM. With an increase of annealing time, further slower decrease of the electrical resistivity follows, which is caused by slight coarsening of the nanocrystalline grains.

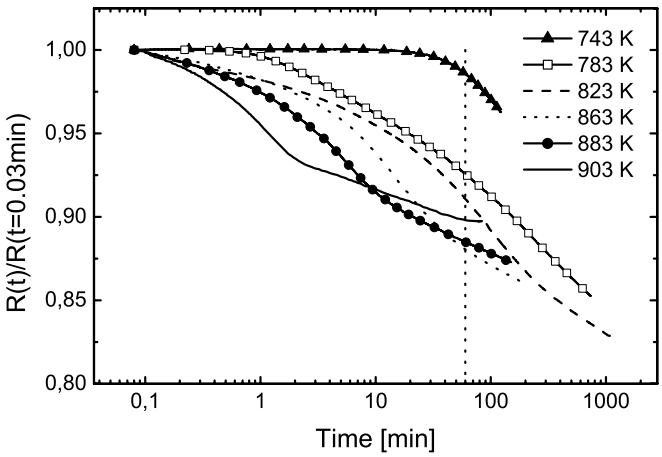

Figure 4. Isothermal time dependence of electrical resistivity at selected annealing temperatures. The dotted vertical line (at 60 min) indicates the crystallization stages for the samples which were selected for further investigations.

Table 1. Results from fine-scale XRD scans on samples annealed at 743, 783 and 883 K for 1 h showing interplanar spacings for the observed bcc structure and the determined average lattice parameter a compared with the lattice parameter of pure α-Fe: all values in nanometres. The fractions of crystallinity v_{cr}(XRD) and v_{cr}(mag) are calculated from the intensities of the first diffraction peak [110] and from the thermomagnetic plots, respectively. The mean grain sizes, d, at different annealing stages are determined from TEM observations.

Plane [hkl]	743 K	783 K	883 K	pure α-Fe
110	2.879	2.872	2.866	
200	2.877	2.870	2.868	
211	2.876	2.870	2.866	
022	2.877	2.871	2.867	
a (nm)	2.877 ± 0.002	2.871 ± 0.002	2.867 ± 0.002	2.866
v_{cr}(XRD) (%)	10 ± 5	35 ± 5	70 ± 5	
v_{cr}(mag) (%)	5 ± 2	26 ± 2	62 ± 2	
d (nm)	<8	10–14	15–20	

According to the above results we have selected three different annealing stages, which have been subjected to more detailed structural characterization. The corresponding samples can be characterized as follows:

(i) the sample annealed at 743 K for 1 h represents an example of a nanocrystalline system with a low fraction of crystalline grains;
(ii) the sample annealed at 783 K for 1 h corresponds to the material in a medium stage of the primary crystallization process and
(iii) the sample annealed at 883 K for 1 h represents a stage where the primary crystallization process is nearly finished.

XRD patterns (figures 5(a), (b)) show at all three annealing temperatures the lines of a bcc crystalline phase only. The corresponding lattice parameter, a, given in table 1, is very close to the value for pure α-Fe (the solubility of Nb in α-Fe is less than 1 at.%). As shown in [23], the crystalline Fe–Nb system may form a supersaturated solid solution with an Nb content of 0–0.56–1.02 at.% and a bcc lattice parameter a of 0.286 63–0.286 77–0.286 97 nm,

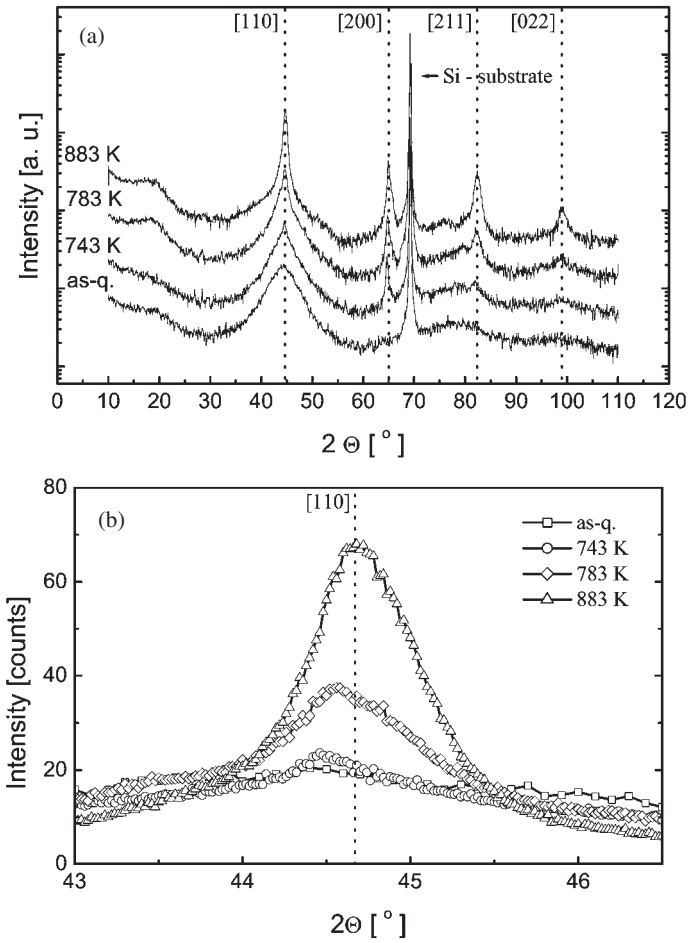

Figure 5. (a) XRD spectra for as-quenched and annealed samples showing the presence of bcc lines only. The dotted lines and indices indicate the positions of the planes for pure α-Fe; the calibration peak at 69.2° originates from the silicon substrate. (b) The evolution of the position of the main peak in the XRD spectra with annealing temperature towards the values corresponding to pure α-Fe (dotted line).

respectively. Therefore, slightly higher values of a observed in the samples with low crystalline fractions, as can be seen in table 1, indicate that such a phase could be present in the early crystallization stages of investigated alloys. In addition, imperfections in the lattice due to the small size of the nanocrystals may play some minor role in the variations of the lattice parameters. With proceeding crystallization at higher temperatures the lattice parameter approaches that of pure α-Fe.

Figures 6(a)–(c) show the dark-field transmission electron micrographs of nanocrystalline $Fe_{80.5}Nb_7B_{12.5}$ samples annealed at the indicated temperatures. The range of grain sizes can be inferred from these images to be about 5–10 nm for the sample annealed at 743 K for 1 h. On the other hand, the annealing at 883 K for 1 h caused the formation of nanocrystalline microstructure with typical dimensions of grains being 15–20 nm. The increase in the mean grain size with an increase of annealing temperature can be seen in table 1, where the corresponding structural data are summarized.

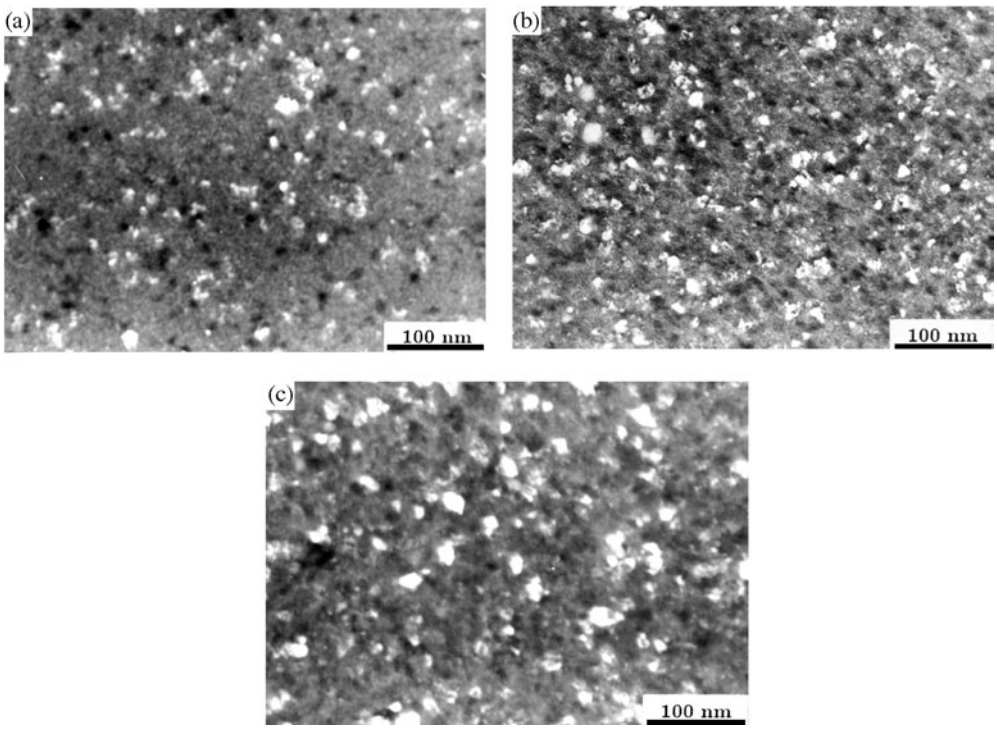

Figure 6. (a)–(c) TEM from the samples annealed at 743, 783 and 883 K, respectively, showing the different sizes of nanocrystalline grains formed at different crystallization stages.

3.2. Magnetic properties

Figure 7 shows the temperature dependences of the magnetization for the amorphous and nanocrystalline samples measured in the temperature range 300–1050 K. The experimental curves for all nanocrystalline samples show behaviour typical for the material containing two ferromagnetic phases. The increase of magnetization in the temperature range above the Curie temperature of the amorphous matrix is due to the presence of nanocrystalline bcc-Fe particles with higher T_c value, which have precipitated during previous annealing treatment. The magnetization of partially crystallized samples grows rapidly when the measuring temperature rises above T_{x1} due to further crystallization, then decreases again and finally vanishes in the vicinity of the Curie temperature of the bcc-Fe phase. The high-temperature thermomagnetic plots allowed us to estimate the volume fraction of crystalline phase to be about 5, 26 and 62% for the samples annealed at 743, 783 and 883 K respectively. These data are collected in table 1.

For partially crystallized samples a distinct kink in $M(T)$ curves is observed at temperatures where the residual amorphous matrix goes from the ferromagnetic to the paramagnetic state. Figure 8 shows the corresponding derivatives of the $M(T)$ dependences with respect to the temperature. The magnetic transition temperature of the residual amorphous matrix, T_c(am), corresponds to the value where the $\delta M/\delta T$ curve displays the minimum. For the samples with low and medium fraction of crystalline phase it is clearly seen that this minimum is shifted to the higher-temperature region as compared with the amorphous sample, indicating the increase of the Curie temperature of the residual amorphous matrix after nanocrystallization. The sample annealed at 743 K exhibits a relatively sharp magnetic

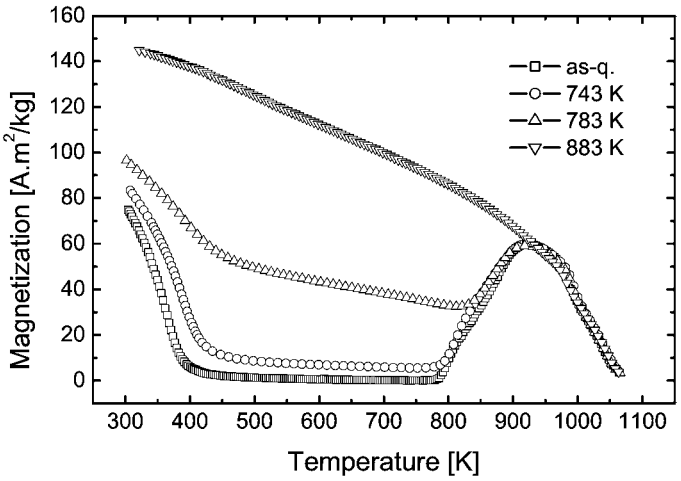

Figure 7. Temperature dependences of magnetization for the as-quenched sample and for the samples annealed at 743, 783 and 883 K, measured at an applied field of 0.3 T.

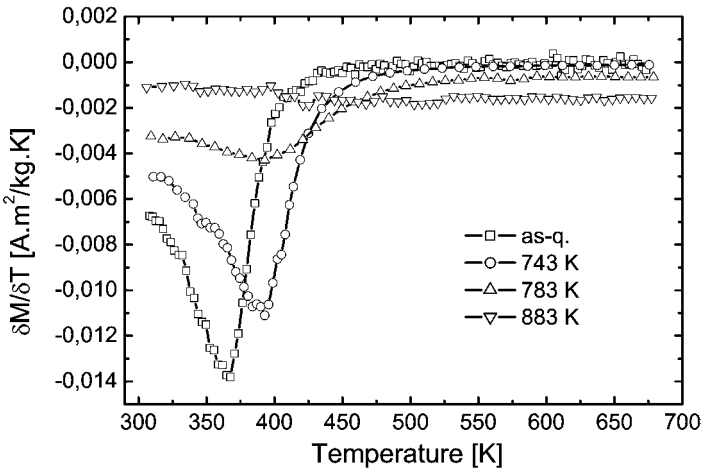

Figure 8. Derivatives of the magnetization curves in the temperature range where the intergranular phase exhibits a transition from the ferromagnetic to paramagnetic state.

transition similar to that of as-quenched amorphous alloy. This transition is however smeared out in the case of the sample annealed at 783 K exhibiting a medium stage of nanocrystallization and it is not visible for the sample annealed at 883 K, that exhibits advanced crystallization. This indicates the more diffuse character of the ferromagnetic–paramagnetic phase transition in the residual amorphous matrix for the specimens containing higher crystalline fractions in accordance with the previous results for FeZrB(Cu) alloys [24].

The soft-magnetic behaviour was investigated by quasi-static hysteresis loop measurements. The coercive field values at room temperature as a function of the annealing temperature are shown in figure 9. The initial magnetic softening is observed for the samples annealed below the crystallization temperature (see the inset in figure 9). This behaviour is attributed to relaxation of the internal stresses, which are connected with the local agglomerations of free volumes trapped in the amorphous structure during rapid quenching.

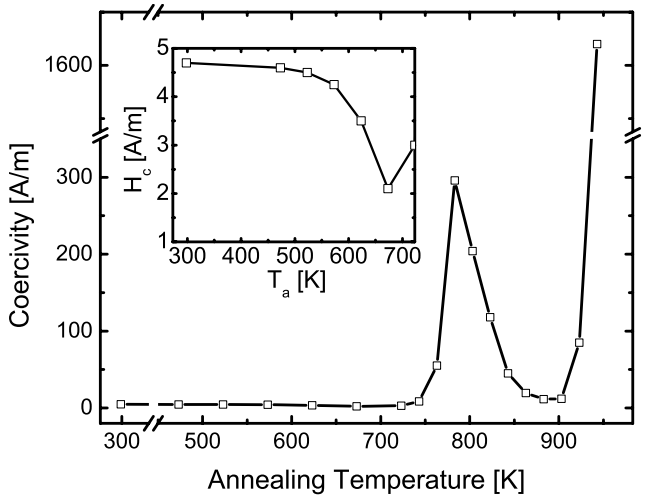

Figure 9. Coercivity versus annealing temperature determined from the hysteresis loops taken at room temperature.

A different behaviour is observed after the partial nanocrystallization. The samples with fairly small fraction of nanocrystals show initially a marked deterioration of soft-magnetic behaviour with an increase of the annealing temperature. The maximum value of the room-temperature coercive field is found for the sample annealed at 783 K, that corresponds to the material in a medium stage of the primary crystallization process. The further increase of annealing temperature results in a decrease of coercive field, i.e. the very good soft-magnetic properties are regained for these advanced nanocrystallization stages. Finally, a rapid increase of coercivity is observed again for annealing temperatures higher than 923 K, which we assume to be caused by the formation of boride phases that show rather high magnetocrystalline anisotropy values.

The first stages of the nanocrystallization process in Nanoperm alloys are very often connected with marked deterioration of soft-magnetic properties [10, 25, 26]. Here the values of T_c(am) are not far above room temperature, and hence this magnetic hardening is believed to be a consequence of the reduced capability of the weak magnetic amorphous matrix to transmit the exchange coupling between nanocrystalline grains. The improvement of soft-magnetic behaviour with higher volume fraction of nanocrystalline phase is explained by the decrease of intergranular distances as well as by the changes in magnetic properties of the matrix, which allow stronger exchange coupling between bcc-Fe nanocrystals.

Figure 10 shows the temperature evolution of the coercive field for two nanocrystalline samples that exhibit the largest and the smallest coercivity values at room temperature. The sample annealed for 1 h at 783 K displays in the temperature range above 300 K a marked magnetic hardening. This is a consequence of less effective intergrain coupling mediated by magnetic matrix, which becomes weaker and weaker with an increase of temperature towards T_c(am). The nanosized grains experience the strongest decoupling when the temperature approaches the Curie temperature of the intergranular amorphous phase. As can be seen in the inset of figure 10, the derivative of $H_c(T)$ with respect to temperature displays there a sharp peak, which coincides well withT_c(am). The coercive field reaches its maximum value slightly above T_c(am) and then decreases. This decrease is due to an increased population of uncoupled grains, which are subjected to significant thermal fluctuation effects [27]. On the other hand,

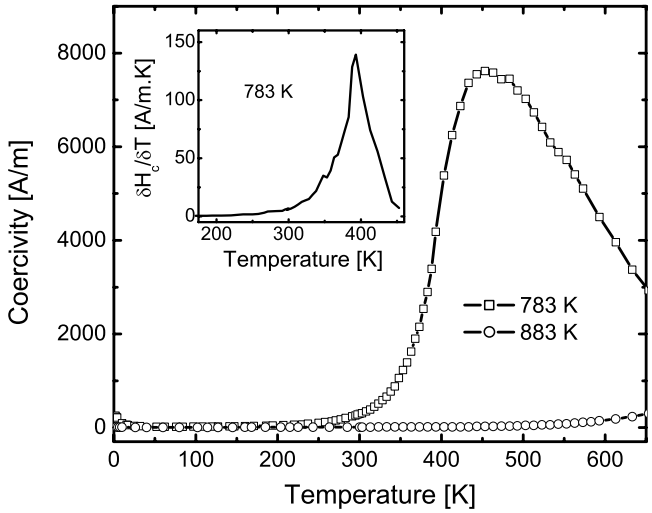

Figure 10. Temperature dependences of coercivity for the samples annealed at 783 and 883 K.

the sample annealed for 1 h at 883 K retains the low value of coercive field to temperatures exceeding 600 K. This indicates that in the samples with advanced degree of crystallinity the good magnetic coupling between the nanocrystals persists to relatively high temperatures.

3.3. ^{57}*Fe Mössbauer study*

Figure 11 illustrates Mössbauer spectra taken at 77 K for selected amorphous and nanocrystalline alloys. The presence of the crystalline phase is reflected by emergence of an additional sextet, which grows when the annealing temperature increases. Each sample has been investigated at different temperatures and the more representative spectra for the samples annealed at 783 and 883 K are shown in figure 12. The different hyperfine parameters were refined by means of the method described in the previous section. The narrow line sextet with hyperfine field value close to that for crystalline bcc-Fe (about 33 T at 300 K) is unambiguously attributed to the Fe atoms located in the inner part of precipitated nanocrystalline bcc-Fe particles. The distributed low-field component corresponds to the Fe atoms located in the residual amorphous matrix whereas the distributed high-field component can be assigned to the Fe atoms present in the crystalline/amorphous interfacial regions. The relative weights of the respective spectral components allowed us to determine the relative fractions of crystalline phase in the investigated samples as a function of annealing temperature: 4% for sample 743 K/1 h, 21% for 783 K/1 h and 45% for 883 K/1 h. These values are systematically found to be smaller than those estimated from x-ray pattern analysis and/or those determined from the thermomagnetic plots. Similar disagreement has also been observed in some other nanocrystalline alloys of this group and its origin was discussed in [28].

The temperature dependences of the mean hyperfine field of the intergranular amorphous phase in selected nanocrystalline specimens are compared with that of the as-quenched amorphous precursor in figure 13. For the sample annealed at 743 K/1 h, the hyperfine field is found to be higher than that of the as-quenched sample, whatever the temperature is. One also observes a significant increase of the Curie temperature, T_c(am), that corresponds to the vanishing of the hyperfine field of the amorphous matrix phase at this early crystallization stage. For the higher annealing temperatures, the presence of a badly resolved kink in the

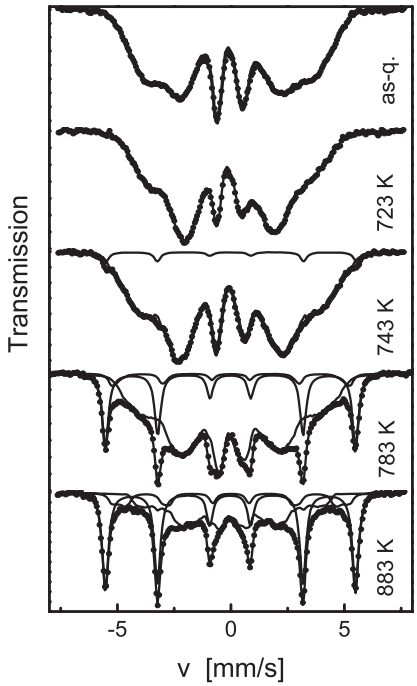

Figure 11. Mössbauer spectra recorded at 77 K on the amorphous alloy and the nanocrystalline alloys obtained after annealing at 723, 743, 783 and 883 K for 1 h. The continuous curves correspond to the different components, as discussed in the text.

corresponding temperature dependences of the mean hyperfine field prevents an accurate estimation of the Curie temperature of the intergranular phase. The temperature range of these measurements was kept well below the crystallization temperature to avoid further amorphous–crystalline transformation. Figure 13 shows that the above temperature limit of our experiment does not allow us to observe the vanishing of the mean hyperfine field of the residual intergranular phase for the samples containing higher volume fractions of nanocrystalline phase.

It is also interesting to follow the evolution of the hyperfine field distributions of the intergranular phase as a function of temperature in order to establish some information on the atomic diffusion process during the two crystallization stages. Figure 14 thus compares the hyperfine field distributions characteristic of the amorphous and nanocrystalline samples at three selected temperatures. As shown in figure 14 for 77 and 300 K, a bimodal behaviour emerges for low-crystalline-fraction nanocrystalline alloy. At these temperatures, no significant low-field (<5 T) contribution is observed. For samples annealed at 783 and 883 K, the distribution spreads out over a broader hyperfine field range, even when the measuring temperature approaches the Curie temperature. Such features are consistent with recent results obtained in the case of some other Fe-based nanocrystalline alloys [18, 24, 29, 30]. The high-field contribution is usually attributed to Fe preferentially neighboured by Fe and B atoms whereas the low-field peak might correspond to Fe preferentially neighboured by Nb atoms. It is important to emphasize that it is also difficult to clearly separate the low magnetic hyperfine fields from the quadrupolar splitting originated from paramagnetic iron sites (an approach was proposed in [30]).

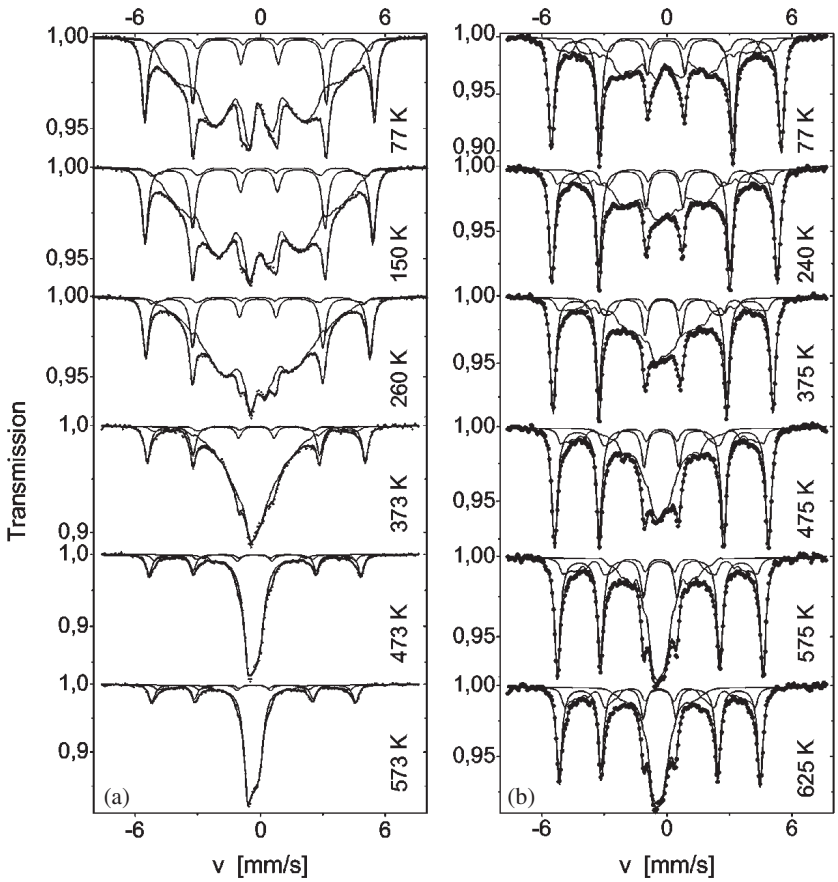

Figure 12. Mössbauer spectra recorded at different temperatures on two nanocrystalline alloys: 783 K (left-hand column) and 883 K (right-hand column) for 1 h. The continuous curves correspond to the different components, as discussed in the text.

3.4. Mechanical properties

Figure 15 shows the evolution of ductile/brittle behaviour with increasing annealing temperature. The value of $\varepsilon_f = 1$ corresponds to ductile specimens, which can be bent through 180° without fracture. If the ribbon fails upon bending, ε_f is smaller than unity and the more brittle the sample is the smaller is ε_f. It is shown that the embrittlement starts around 623 K, i.e. still in the amorphous state, prior to the formation of the first nanocrystals. The relative strain at fracture drops rapidly with a subsequent increase of annealing temperature and the further increase of T_a above 773 K has almost no influence on ε_f. Clearly, the two-phase alloys with the nanocrystalline bcc-Fe grains embedded in the amorphous matrix phase exhibit poor bending ductility, irrespective of the amount of crystallinity. This observation is in good agreement with our previous results reported for FeCuNbSiB (Finemet) alloys [13]. However, the embrittlement of Finemet alloys started to develop already when the annealing temperatures exceeded 473 K, and hence they show a substantial degree of embrittlement already far below the crystallization temperature.

Similar conclusions about the embrittlement level versus annealing temperature can be drawn from the ball punch tests. As can be seen from figure 15, an elongation of about 2.7%

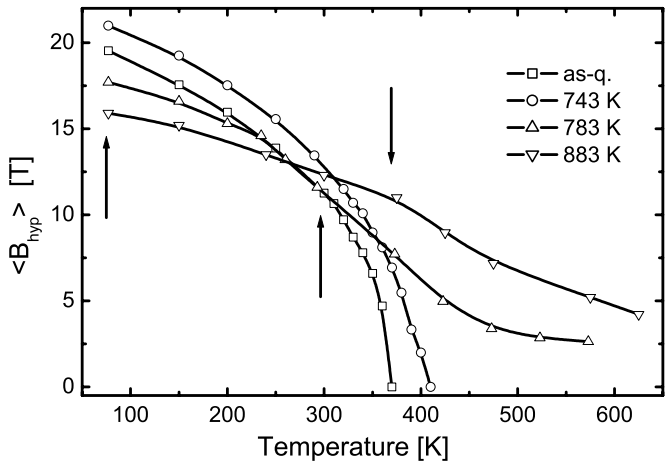

Figure 13. Temperature evolution of the mean hyperfine field of the as-quenched amorphous alloys and of the intergranular phase of the nanocrystalline alloys obtained after annealing at 743, 783 and 883 K for 1 h.

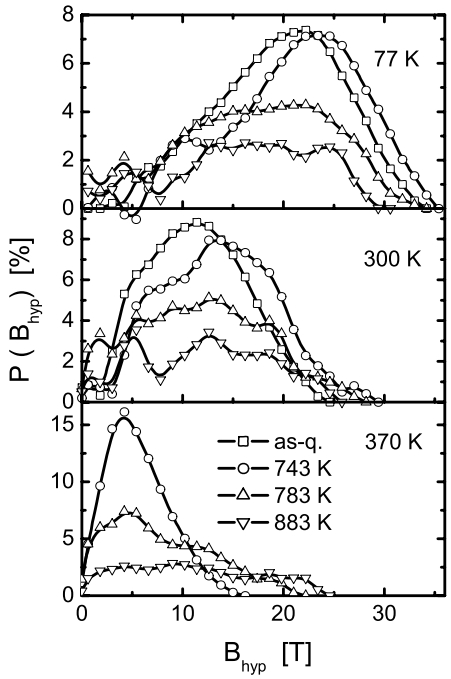

Figure 14. Hyperfine field distributions, obtained at 77, 300 and 370 K, of the as-quenched amorphous alloys and of the intergranular phase of the nanocrystalline alloys obtained after annealing at 743, 783 and 883 K for 1 h.

has been observed for the as-quenched amorphous sample. The embrittlement starts around 623 K. The main loss of ductility occurs between 623 and 723 K. However, in contrast to ε_f, which remains about unchanged above ∼773 K, the ball punch tests indicate a slow but continuous decrease in ε_{BP} between 773 and 873 K to ∼0.4%. The reason of this difference is a better resolution of the ball punch test for the brittle specimens.

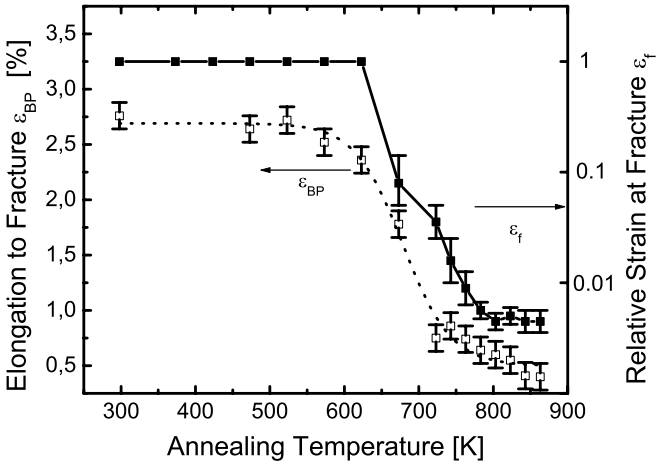

Figure 15. The relative strain at fracture and the elongation at fracture as a function of annealing temperature for amorphous and nanocrystalline $Fe_{80.5}Nb_7B_{12.5}$.

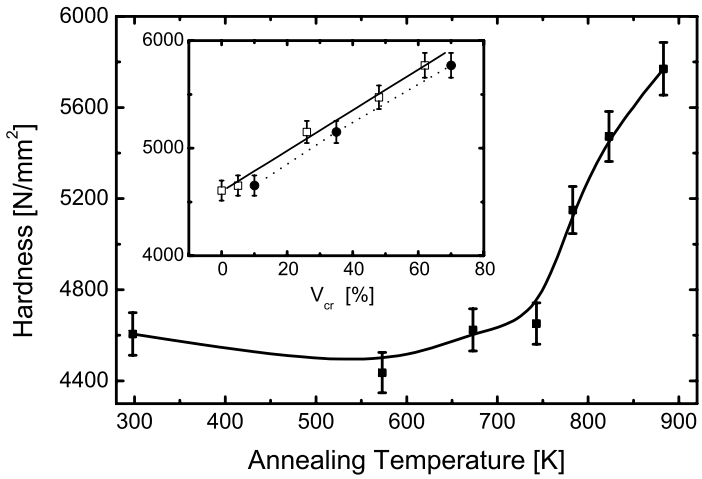

Figure 16. Hardness as a function of annealing temperature for amorphous and nanocrystalline $Fe_{80.5}Nb_7B_{12.5}$ (the inset shows the hardness versus the fraction of crystallinity: (i) ——v_{cr} determined from thermomagnetic plots, (ii) · · · · · ·v_{cr} determined from XRD).

The microhardness tests have been used as an additional method to characterize the mechanical properties of the investigated alloy. Figure 16 shows the variation of hardness with temperature. In contrast to the ductility as characterized by the bending and ball punch tests, the hardness is rather insensitive to the structural relaxation prior to crystallization. Microhardness starts to increase markedly with the precipitation of nanocrystalline particles and, as can be seen from the inset in figure 16, the increase shows an almost linear dependence on the volume fraction of crystalline grains (v_{cr} was determined from thermomagnetic plots and XRD data). We note that for the used load of 1 N the light optical micrographs have not revealed any material pile-up or cracking morphologies around the indentations.

4. Discussion

The structure of the sample in its pre-crystallization stage may be considered chemically inhomogeneous on the atomic scale, containing the regions (clusters) rich in Fe–Nb–B and regions with a smaller amount of Nb in the vicinity of Fe atoms. The origin of such clusters can be related to the medium-range order (MRO) domains (1–2 nm) that were observed by Nakamura *et al* [31] in the sputter-deposited thin films of similar composition as compared with our rapidly quenched alloy. As the clusters richer in Nb are more stable against crystallization, the first crystalline nuclei may be formed from the Fe clusters depleted in Nb, leading to the formation of nanocrystals containing a supersaturated solid solution of Nb in α-Fe, as suggested by XRD spectra for the samples annealed at 743 and 783 K. More stable regions enriched in Fe–Nb crystallize after longer annealing time or at higher temperatures. This effect may be responsible for the observed two-stage character of the primary crystallization process as shown in figures 1–3.

In the case of the samples that exhibit advanced stages of nanocrystallinity, the increased diffusion of Nb from the nanocrystalline grains at higher temperatures combined with its insolubility in Fe may lead to its spreading over the remaining amorphous matrix without forming a significant concentration gradient of Nb at the interface between the nanocrystals and the remaining amorphous matrix. This may be responsible for further enhancement of stability of the remaining Fe–Nb–B amorphous matrix against crystallization: the crystallization reaction proceeds over an uncommonly large temperature interval of $\sim$100 K.

The activation energy for the crystallization process is quite high, $\sim$400 kJ mol^{-1}, and the Avrami parameter decreases smoothly throughout the whole reaction from $\sim$4 to $\sim$2.5, suggesting continuous nucleation and slight growth of nanocrystals by a unique mechanism [32]. The observed high activation energy is in agreement with the assumption about increased mobility of Nb atoms at higher temperatures.

The chemical composition and the properties of the amorphous matrix that surrounds the growing nanocrystallites change during the crystallization process. It has been reported for several nanocrystalline alloy systems that after partial devitrification the increase in T_c(am) of residual matrix takes place with respect to the value expected from the known compositional dependence for the bulk amorphous materials [24,33]. The non-homogeneity of the amorphous phase arising from the diffusion during nanocrystallization [34] and the penetration of the exchange field caused by the nanocrystallites into the residual amorphous matrix [33] have been suggested as an origin of this behaviour. In our previous study, the magnetic and hyperfine parameters of the intergranular amorphous phase in the $Fe_{80.5}Nb_7B_{12.5}$ alloy annealed for 1 h at 783 K were compared with those of the analogous single-phase melt-spun material [35]. Such an approach has clearly indicated that in the above nanocrystalline specimen the major role in the enhancement of T_c(am) is played by the penetrating exchange fields originating from the nanocrystalline grains. As a consequence of such penetrating fields, the mean hyperfine field of the residual intergranular phase in the samples containing higher volume fractions of nanocrystalline phase retains non-zero values at high temperatures (see figure 13). This has a beneficial effect on the magnetic softness of these nanocrystalline specimens [36]. Hence, the nanograins in the sample annealed for 1 h at 883 K remain well magnetically coupled in the whole temperature range investigated.

The ductility problem in various nanocrystalline materials has been reviewed in the recent articles of Koch *et al* [37, 38]. It has been shown that these materials can exhibit wide variations in ductility depending on the constituent phases, grain sizes and processing methods. An example of a nanocrystalline system where the nanocrystalline grains coexist with an amorphous matrix phase, which shows simultaneously high strength and good ductility,

is the group of the Zr–Al–Cu–Pd–(Fe) alloys synthesized by Inoue *et al* [39]. It is assumed that good ductility in these nanocrystalline alloys is due to the reentrance of free volumes into the remaining amorphous phase caused by quenching from the supercooled liquid region. On the other hand, the Fe-based nanocrystalline soft-magnetic materials are brittle and their embrittlement develops already during the heat treatment in the amorphous phase, i.e. before the nanocrystallization. For a variety of amorphous alloys, the first stages of embrittlement due to relaxation annealing at temperatures well below the crystallization temperature are accompanied by an increase of density [40]. This indicates that this low-temperature embrittlement is closely correlated with a decrease of excess free volume, which is retained from quenching.

The amount of excess free volume in the amorphous phase seems to also play the key role in the ductile/brittle transformation for the present system. The comparison of figures 9 and 15 clearly shows that the decrease of coercivity in the amorphous phase and the loss of ductility develop in the same temperature range below the crystallization temperature. Hence, at this stage of heat treatment, the annealing out of excess free volume is believed to be a reason for the observed magnetic softening and the embrittlement. In this respect a modified heat treatment, which allows us to preserve more free volume in the residual amorphous phase, would be beneficial for the ductility. We plan to carry out the related experiments in the future.

The increase of heat treatment temperature above the crystallization temperature and the subsequent amorphous–crystalline transformation has only a small influence on the embrittlement level in investigated samples. This is in contrast to the microhardness, which exhibits a strong sensitivity to the amount of the crystalline fraction transformed during the annealing process. A similar increase of hardness due to the uniform distribution of ultrafine crystalline particles has also been observed for some other nanocrystalline systems [39,41,42]. A simple approach to describe the observed linear relationship between the hardness and the volume fraction of crystalline phase that takes into account a rule of mixtures, $H_v = v_{am} H_{v,am} + v_{cr} H_{v,cr}$, where v_i and $H_{v,i}$ denote the volume fraction and the hardness of the respective phase, has been suggested by Eckert *et al* [42]. Such an empirical approach allows us to treat the material as a two-phase system, where both phases contribute to the overall hardness of the material. This simple rule, however, does not take into consideration the effects of amorphous–crystalline interfaces and the changes of the chemistry of constituent phases during the heat treatment process. Nevertheless, it describes the experimental data (inset in figure 16) quite well.

5. Conclusions

Structural, magnetic and mechanical properties of $Fe_{80.5}Nb_7B_{12.5}$ alloys have been investigated in the same series of amorphous and nanocrystalline samples characterized by different microstructure. The results can be summarized as follows.

- The experimental data obtained by DSC calorimetry, magnetization and electrical resistivity measurements have confirmed a two-stage nature of the primary crystallization process in the investigated alloy.
- The results obtained by a combination of static magnetic measurements and Mössbauer spectrometry indicate a higher degree of structural and magnetic inhomogeneity of the residual amorphous phase after nanocrystallization, resulting in a more diffuse character of the ferromagnetic–paramagnetic phase transition for the specimens containing higher fractions of nanocrystalline particles, in agreement with the previous works.
- A deterioration of the soft-magnetic behaviour takes place with the formation of nanocrystalline particles for the samples exhibiting lower fractions of crystallinity.

The good soft-magnetic properties are regained for the samples showing advanced nanocrystallization stages.

- The heat-treated amorphous $Fe_{80.5}Nb_7B_{12.5}$ alloy shows better resistance against the embrittlement as compared with Finemet. The transition from ductile to brittle behaviour develops predominantly in an amorphous phase just before crystallization and the subsequent crystallization causes only slight changes in the embrittlement level.
- The ductility and coercivity in the amorphous phase start to decrease in the same temperature range, indicating that the microstructural changes associated with the annealing out of the excess free volume could be responsible for the observed magnetic softening and the embrittlement in an amorphous phase.
- In contrast to the ductile/brittle transition, the hardness shows only minor changes caused by structural relaxation processes before crystallization but its value increases proportionally to the volume fraction of precipitated nanocrystalline grains.

Acknowledgments

This work was supported by the Volkswagen Foundation under project No VW-I/75961. The authors also acknowledge the partial support of the France–Slovak (CNRS–SAS) exchange programme, Slovakian VEGA (projects 2/1149 and 2/2038) and COST 523.

References

[1] Yoshizawa Y, Oguma S and Yamaguchi K 1988 *J. Appl. Phys.* **64** 6044
[2] Suzuki K, Makino A, Inoue A and Masumoto T 1991 *J. Appl. Phys.* **70** 6232
[3] Makino A, Hatanai T, Inoue A and Masumoto T 1997 *Mater. Sci. Eng.* A **226–8** 594
[4] Herzer G 1990 *IEEE Trans. Magn.* **26** 1397
[5] Herzer G 1995 *Scr. Metall. Mater.* **33** 1741
[6] Hernando A, Vasquez M, Kulik T and Prados C 1995 *Phys. Rev.* B **51** 3581
[7] Suzuki K and Cadogan J M 1998 *Phys. Rev.* B **58** 2730
[8] Vázquez M, Marín P, Davies H A and Olofinjana A O 1994 *Appl. Phys. Lett.* **64** 3184
[9] Hernando A and Kulik T 1994 *Phys. Rev.* B **49** 7094
[10] Škorvánek I and O'Handley R C 1995 *J. Magn. Magn. Mater.* **140–144** 467
[11] Gomez-Polo C, Holzer D, Multigner M, Navarro E, Agudo P, Hernando A, Vazquez M, Sassik H and Grössinger R 1996 *Phys. Rev.* B **53** 3392
[12] Suzuki K, Cadogan J M, Sahajwalla V, Inoue A and Masumoto T 1997 *Mater. Sci. Forum* **235–238** 765
[13] Škorvanek I and Gerling R 1992 *J. Appl. Phys.* **72** 3417–22
[14] Škorvánek I, Gerling R, Graf T, Fricke M and Hesse J 1994 *IEEE Trans. Magn.* **30** 548
[15] Allia P, Barico M, Knobel M, Tiberto P and Vinai F 1993 *Phil. Mag.* B **68** 853
[16] Allia P, Tiberto P, Barico M, Knobel M and Vinai F 1994 *IEEE Trans. Magn.* **30** 4797
[17] Teillet J and Varret F Mosfit program, University of Le Maine
[18] Miglierini M and Grenèche J-M 1997 *J. Phys.: Condens. Matter* **9** 2303
Miglierini M and Grenèche J-M 1997 *J. Phys.: Condens. Matter* **9** 2321
[19] Gerling R and Wagner R 1982 *J. Nucl. Mater.* **107** 311
[20] Schimanski F P, Gerling R and Wagner R 1991 *Mater. Sci. Eng.* A **133** 328
[21] Suzuki K, Cadogan J M, Dunlop J B and Sahajwalla V 1995 *Appl. Phys. Lett.* **67** 1369
[22] Mat'ko I, Duhaj P, Švec P and Janičkovic D 1994 *Mater. Sci. Eng.* A **179/180** 557
[23] *Landolt–Börnstein New Series* 1971 vol 6, ed K H Hellwege and A H Hellwege (Berlin: Springer)
[24] Garitaonandia J S, Schmool D S and Barandiaran J M 1998 *Phys. Rev.* B **58** 12 147
[25] Idzikowski B, Baszynski J, Škorvánek I, Eckert D and Müller K-H 1998 *J. Magn. Magn. Mater.* **177–181** 941
[26] Kopcewicz M, Grabias A, Škorvánek I, Marcin J and Idzikowski B 1999 *J. Appl. Phys.* **85** 4427
[27] Hernando A, Marín P, Vázquez M, Barandiarán J M and Herzer G 1998 *Phys. Rev.* B **58** 366
[28] Lécaudé N, Perron J C, Randrianantoandro N and Greneche J M 1999 *Mater. Sci. Forum* **312–314** 487
[29] Greneche J-M, Miglierini M and Slawska-Waniewska A 2000 *Hyperfine Interact.* **126** 27
[30] Miglierini M, Škorvánek I and Greneche J-M 1998 *J. Phys.: Condens. Matter* **10** 3159

[31] Nakamura M *et al* 1994 *Mater. Sci. Eng.* A **179/180** 487
[32] Krištiaková K and Švec P 2001 *Scr. Mater.* **44** 1275
[33] Hernando A, Navaro I and Goria P 1995 *Phys. Rev.* B **51** 3281
[34] Yavari R 1995 *Nanostructured and Non-Crystalline Materials* ed M Vazquez and A Hernando (Singapore: World Scientific) p 35
[35] Škorvánek I, Kováč J and Greneche J-M 2000 *J. Phys.: Condens. Matter* **12** 9085
[36] Suzuki K and Cadogan J M 1999 *J. Appl. Phys.* **85** 4400
[37] Koch C C and Malow T R 1999 *Mater. Sci. Forum* **312–314** 565
[38] Koch C C, Morris D G, Lu K and Inoue A 1999 *MRS Bull.* **24** 54
[39] Inoue A, Fan C and Takeuchi A 1999 *Mater. Sci. Forum* **307** 1
[40] Gerling R, Schimansky F P and Wagner R 1990 *Int. J. Rapid Solidif.* **5** 137
[41] Varga L K, Bakos E, Kiss L F and Bakonyi I 1994 *Mater. Sci. Eng.* A **179/180** 567
[42] Eckert J, Reger-Leonhard A, Weiß B and Heilmaier M 2001 *Mater. Sci. Eng.* A **301** 1